JOURNAL OF MATERIALS SCIENCE 31 (1996) 2879–2883

Finite element modelling of interfacial failure in model carbon fibre–epoxy composites

R. B. NATH, D. N. FENNER
Department of Mechanical Engineering, King's College London, Strand, London WC2R 2LS, UK.

C. GALIOTIS
Department of Materials, Queen Mary & Westfield College, Mile End Road, London E1 4NS, UK.

Finite element analysis has been used to model a single unsized carbon fibre embedded in an epoxy matrix subjected to tensile loading. The predicted fibre strain distribution is compared with experimental data, obtained using the technique of laser Raman spectroscopy, for a number of incremental applied strain levels. Good correlation is obtained on the assumption that the prevailing mode of interfacial failure in the composite involves a conical matrix crack initiating at the fibre end. The geometry of the matrix crack is estimated on the assumption that the crack propagates in a self-similar manner.

1. Introduction

When a fibre reinforced composite specimen is loaded, most of the load is transferred via the matrix to the fibre. Due to the difference in the elastic moduli of the fibre and matrix, shear stresses are induced at the fibre–matrix interface. The axial strain and the shear stress at the fibre–matrix interface are termed the fibre strain and the interfacial shear stress (τ_{rz}), respectively.

Theoretical predictions of the fibre strain and τ_{rz} distributions along the interface have been made by several authors, notably Cox [1], for the case where both matrix and fibre are assumed to be linear elastic and where the fibre–matrix interface remains intact. In reality, however, as the tensile loading on the specimen increases, the shear stress at the interface reaches a critical value, termed the interfacial shear strength for the system. Beyond this point one or more of the following modes of interfacial failure is observed experimentally [2–9]:

Mode α: matrix yielding at the intact interface. This mode has been observed to occur in aramid fibre–epoxy matrix systems [2, 4].
Mode β: a crack initiates at the fibre end and propagates along the interface. Frictional stress transfer between the fibre and matrix may take place across the crack faces. This failure mode has been observed to occur in glass fibre systems [10].
Mode γ: a conical crack initiates at the fibre end and propagates into the matrix at an angle to the axis of the fibre. The failure mode has been observed in carbon fibre systems [11–13].

The fibre strain distribution along the interface has been measured experimentally for crystalline fibre–matrix systems using the technique of laser Raman spectroscopy (LRS) [2, 3, 5, 7]. This technique relies on the fact that the Raman frequency of the atomic vibrations of crystalline reinforcing fibres, such as aramid or carbon, depends on the axial strain, e_f, in the fibre. Unique Raman frequency versus e_f calibration curves, produced for each type of fibre, are used to convert the measured Raman frequency variation along an embedded fibre to an axial strain distribution in the fibre. The corresponding distribution of the interfacial shear stress, along the length of the fibre, deduced by means of a simple force balance for an infinitesimal length of fibre [2, 3, 5, 7] is given by

$$\tau_{rz} = -\frac{1}{4} D E_f \frac{de_f}{dz} \quad (1)$$

where r and z are the radial and axial directions, respectively, D is the diameter of the fibre and E_f is the elastic modulus of the fibre. The τ_{rz} distribution is obtained by fitting a cubic spline to the experimental fibre strain data and employing Equation (1).

The fibre strain distribution has been obtained experimentally for both continuous and discontinuous fibre–epoxy composites [5]. For discontinuous aramid fibre-epoxy composites, the τ_{rz} in the elastic region is maximum at the ends and decays to zero at the middle of the fibre [4]. When interfacial failure occurs at the fibre ends, the τ_{rz} drops to zero at these points, builds to a maximum and finally decays to zero at the middle of the fibre [5]. The distance over which the τ_{rz} builds to its maximum value from the fibre ends can be used to estimate the extent of interfacial debonding in each case. In certain aramid fibre–epoxy composites [6], the fibre strain distribution after interfacial failure, appears trapezoidal in shape and the maximum τ_{rz} reaches a value of approximately 45 MPa at a certain distance from the fibre end and then decays to zero at the fibre centre. This behaviour

0022–2461

is attributed to resin or interphase plasticity due to the high von Mises stresses developed near the fibre ends and has been modelled by Guild *et al.* [4] using finite element (FE) analysis.

The micromechanics of reinforcement during fibre fragmentation of a high-modulus carbon fibre–epoxy system under tensile loading has been studied by Melanitis *et al.* [3]. The fibre strain distribution was monitored at each level of load until full fragmentation occurred. After fracture, the fibre strain was found to build from the tips of the fibre fractures reaching a maximum value in the middle of each fragment. The shape of the derived τ_{rz} distribution indicates that interfacial failure in these systems initiates at the fibre fracture. The average maximum value of the τ_{rz} increases to approximately 40 MPa at an applied strain, e_{app} of 1.8% (full saturation) and then gradually decreases with further strain increments.

The measured fibre strain distribution along a short high modulus carbon fibre–epoxy composite [9] suggests that some sort of interfacial failure initiates at the fibre ends just prior to fibre fracture. The strain–energy release rate required for interfacial failure is reached prior to first fibre fracture and, therefore, unstable propagation of an interfacial crack is likely to take place at the same time as fibre fracture [9].

In this paper, results obtained using a FE model of a single unsized carbon fibre–epoxy composite, incorporating a Mode γ conical crack, are compared with experimental data obtained using the LRS technique [3]. The crack geometry for which the predicted fibre strain distribution correlates best with the experimental data is thereby established.

Experimental observation of conical cracks in carbon fibre reinforced systems is generally very difficult to perform optically. Scanning Electron Microscopy evidence of conical cracks in this type of system are reported elsewhere [12], and also by other authors [13].

2. Experimental measurements

The model composite employed comprises a single continuous high modulus carbon fibre embedded in an epoxy resin. The fibres, supplied by Courtaulds Graphil plc, were approximately 6.5 μm in diameter and a Ciba Geigy MY750/HY951 epoxy resin was used. Full details of the manufacturing procedure is given in [3]. The elastic modulus of the fibres, measured in the axial direction, was 390 GPa and that of the matrix was 2.6 GPa.

The composite is subjected to incremental tensile loading up to full fragmentation of the embedded fibre. Using the technique of LRS, the fibre strain distribution along the length of the fibre is obtained for various levels of the applied strain, e_{app}. The experimental strain data was obtained from a number of fibre fragments having lengths greater than the critical length. It is to the raw experimental data that matching was made, so an inherent scatter in the data is observed (Figs 4(a–c)). This is inevitably due to the normal experimental error associated with the LRS technique.

Raman spectra were taken with the 514.5 nm line of an Argon-ion laser at an incident power of less than 2 mW. The laser beam was focused to a 2 μm spot on the fibre using a modified Nikon microscope and the Raman back-scattered light was analysed by a SPEX 1877 triple monochromator. Further details of the experimental set up are given in [3].

3. Finite element model

Preliminary experimental studies have shown that, of the three possible modes of interfacial failure described above, the Mode γ failure is the most likely to occur in high modulus carbon–epoxy systems [12].

The axisymmetric FE model of the Mode γ failure (see Fig. 1) includes a conical-shaped crack and covers only one quarter of the diametral section, due to the symmetry of the problem (Fig. 2). The matrix is assumed to be linear elastic and isotropic and the fibre is assumed to be linear elastic and transversely isotropic (See Table I for material properties). The mesh consists of 6-node triangular and 8-node quadrilateral axisymmetric elements. The loading takes the form of a uniform displacement imposed on those nodal points lying on the end face of the composite. The geometry of the matrix crack is defined in terms of its orientation, ϕ, with respect to the fibre axis and its length, a. The aim was to find the crack geometry for which the corresponding fibre strain distribution correlated best with the experimental data. The FE meshes were generated using FEMGEN/FEMVIEW and the solutions were obtained using ABAQUS.

4. Results and discussion

The fibre strain distribution obtained from the FE model of the Mode γ interfacial failure (see Fig. 3a), exhibits the characteristic *S*-shape in the take-up region [3]. This *S*-shape has been observed in the experimental fibre strain data, and was found to become more pronounced as the applied strain on the composite was increased. It was also found that the τ_{rz} reaches a maximum value at a finite distance from the fibre end (see Fig. 3b), a feature also observed in the experimental data.

The FE predictions for the displacements in the model reveal that the crack opens up under the influence of the tensile loading. It follows that there cannot be any frictional load transfer across the crack faces for this mode of interfacial failure. Load transfer by a frictional mechanism, as has been proposed by

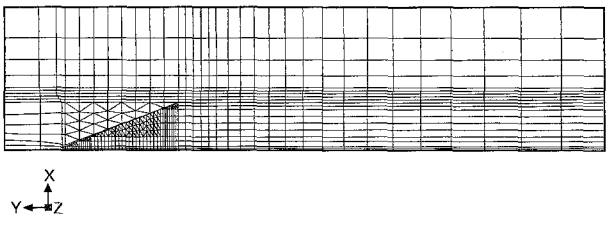

Figure 1 Axisymmetric FE mesh of a single fibre composite with Mode γ interfacial failure.

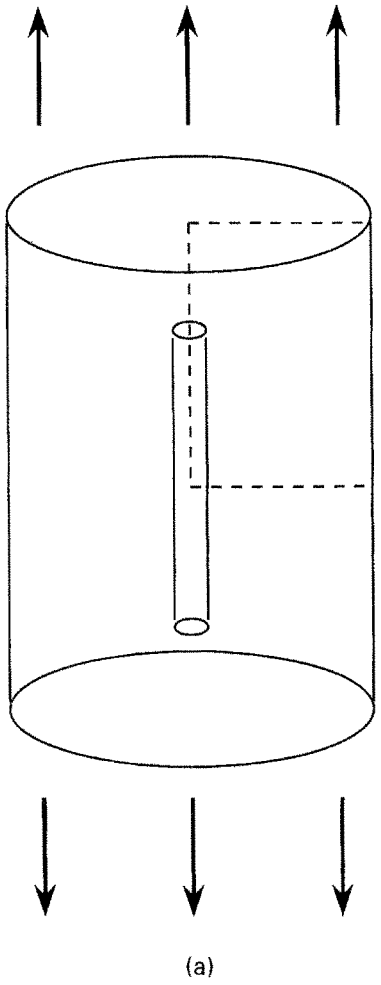

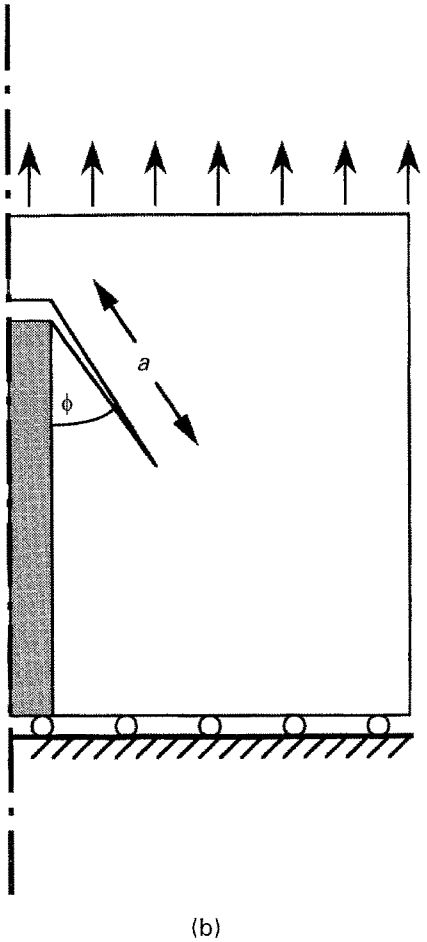

Figure 2 (a) Specimen geometry (b) Axisymmetric section showing Mode γ interfacial failure.

TABLE I Material properties

	Carbon fibre	MY750/HY951 Matrix
Axial tensile modulus	390 GPa	2.6 GPa
Transverse modulus	20 GPa	2.6 GPa
Axial tensile strength	3.2 GPa	78 MPa
Axial fracture strain	0.8%	4.2%
Axial Poissons ratio	0.22	0.36
Transverse Poissons ratio	0.03	0.36

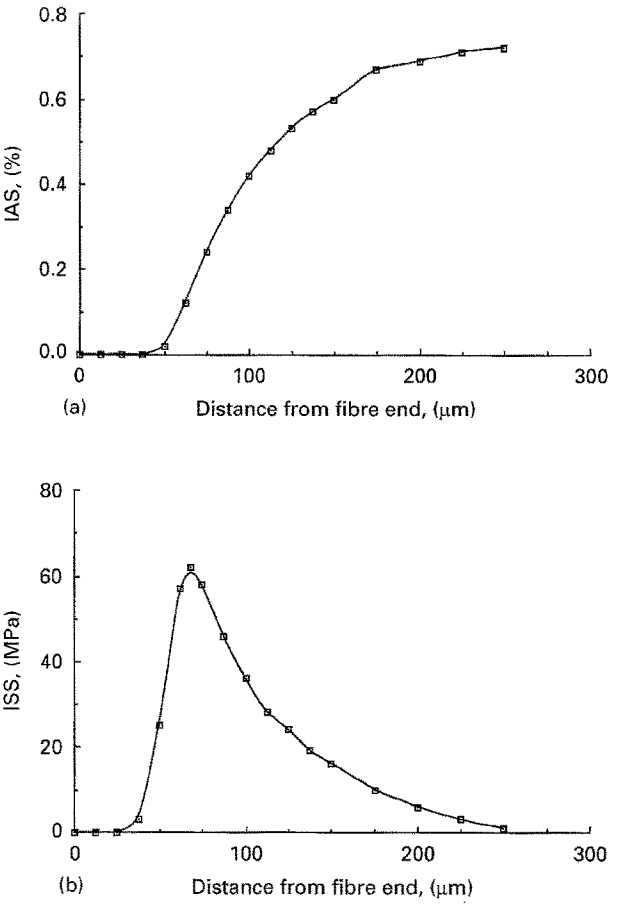

Figure 3 (a) FE predicted fibre strain distribution along fibre for $\phi = 6°$; $e_{app} = 1.05\%$ (b) FE predicted τ_{rz} distribution along fibre for $\phi = 6°$; $e_{app} = 1.05\%$.

Piggott [14] for Mode β type interfacial failure, would necessarily require a closing-up of the crack in order that the crack faces may come into sliding contact with one another.

To investigate the influence of the stress concentration at the crack tip on the interfacial stresses, the crack tip was blunted. The τ_{rz} and fibre strain distributions for the modified FE model were found to be unchanged showing that the interfacial load transfer mechanism is insensitive to events local to the crack tip. Since in the present analysis, the matrix has been modelled as linear elastic, account of the crack tip plastic zone has not been taken. However, insensitivity of the crack tip stress state overcomes this problem, and hence the stress state predicted by the present analysis is valid in the region around the fibre, but not in the localized crack tip region.

It is thought that there exists an interphase region between fibre and matrix whose elastic properties are intermediate between those of the two materials [15]. To investigate the effect of such a region, the FE model was modified to include an interphase whose elastic modulus and Poisson's ratio are quadratic functions of radial distance from the fibre axis. Such elastic property variations are thought to be representative of actual interphasial regions [15]. The interphase modelled was 1 μm thick, an overestimate of the real thickness made necessary by the limitations of the FE model. The effect on the fibre strain and τ_{rz} distributions was found to be negligible. A fuller description of the interphase and the variations in elastic modulus and Poissons ratio are given in Appendix A.

The geometric parameters which were found to have the greatest effect on the fibre strain and τ_{rz} distributions, are the angle of orientation, ϕ, of the crack and the crack length, a. In order to establish the geometry of a matrix crack in an actual composite specimen, the combination of these two crack geometry parameters was found that yielded a fibre strain distribution that correlated best with that obtained by experiment, for a given level of applied strain. For $e_{app} = 1.05\%$ these parameters were found to be $\phi = 21^\circ$ and $a = 101$ mm. When the length of the matrix crack was increased, whilst keeping the crack angle constant, good correlation with the experimental fibre strain data was achieved for applied strains of 1.05%, 1.15% and 1.35% (see Fig. 4(a–c)). For $e_{app} = 1.05\%$ there was also fairly good correlation between the FE and experimental results for the τ_{rz} distribution, as shown in Fig. 5.

The assumption of linear elastic behaviour of the matrix provides FE stress/strain predictions which are valid only if the von Mises stress at any point in the matrix does not exceed the tensile yield strength of the matrix (refer Table I). In the present analysis, the region of matrix adjacent to the fibre supports stresses below the tensile yield stress, for the given levels of applied strain. This is predominantly because the crack tip is the site for the stress concentration in the system.

It has been observed in many studies of the propagation of interfacial and matrix cracks, in various composite systems, that they initiate at a certain angle to the fibre axis, but subsequently turn towards the interfacial region [10, 11]. Matrix cracks have also been observed to bifurcate or even trifurcate at certain critical points within a composite, thus making the problem even more complex [10, 11].

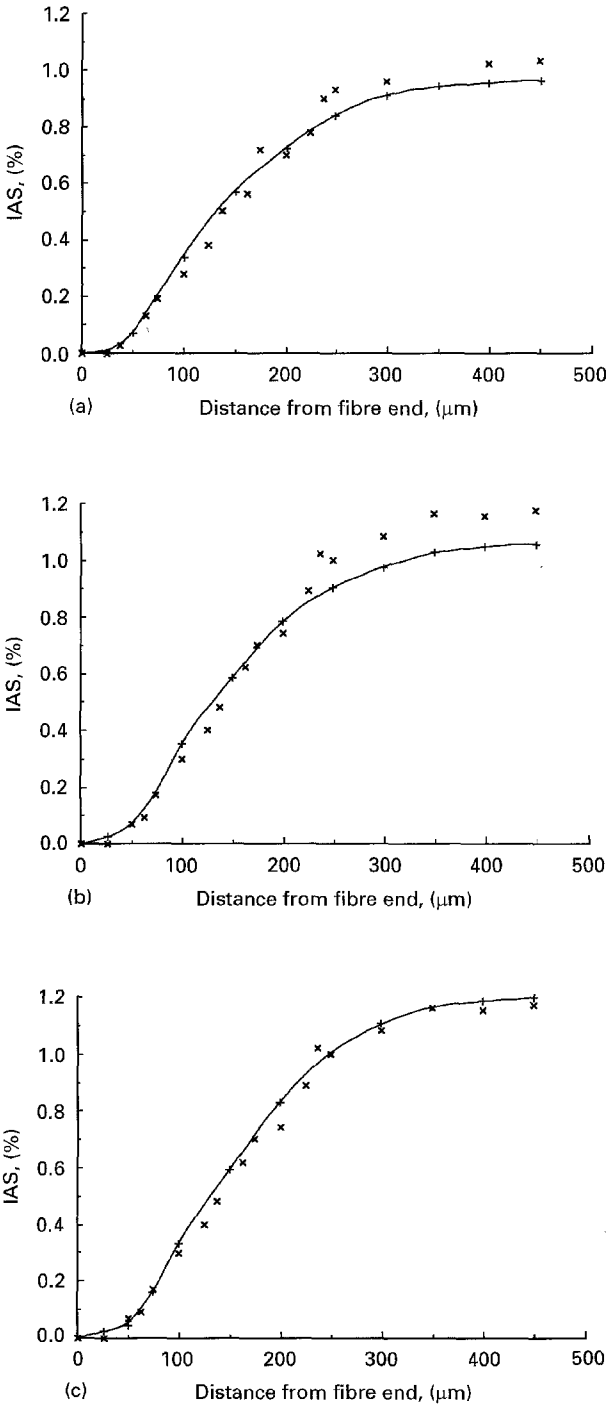

Figure 4 (a) Fibre strain distribution along fibre for $\phi = 21^\circ$; $e_{app} = 1.05\%$ where (+) FE results and (×) experimental results (b) Fibre strain distribution along fibre for $\phi = 21^\circ$; $e_{app} = 1.15\%$ where (+) FE results and (×) experimental results (c) Fibre strain distribution along fibre for $\phi = 21^\circ$; $e_{app} = 1.35\%$ where (+) FE results and (×) experimental results.

5. Conclusions

Finite element analysis has shown that experimental results obtained for the fibre strain distribution in a carbon fibre–epoxy composite are consistent with a Mode γ type of interfacial failure. In this mode of failure, a conical matrix crack initiates at the fibre end and propagates into the matrix. The angle of propagation was estimated to be 21° to the longitudinal fibre axis. It is likely that the conical crack initiates at this angle so as to maximize the strain–energy release rate after the end face of the fibre has debonded.

Appendix: Concept of the boundary interphase

In the interaction between a fibre and matrix, a rather complex situation develops in which a third phase is thought to exist. This third phase is known as the interphasial region, and it extends between the fibre and matrix.

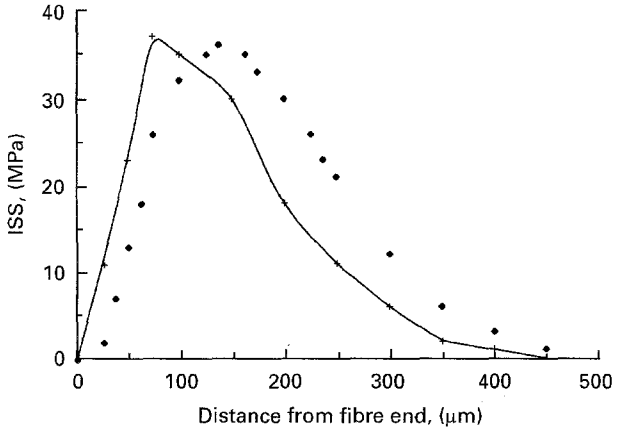

Figure 5 τ_{rz} distribution along fibre for $\phi = 21°$; $e_{app} = 1.05\%$ where (+) FE results and (◆) experimentally derived results.

It is the result of physio–chemical interaction between fibre and matrix and may be simply described as a restricted zone where impurities and air bubbles are concentrated and microcracks have developed. In this layer, the macromolecules of the matrix show a constraint of their degree of freedom to polymerize, especially for their sidesubchains, since they are neither totally free to rotate close to the interface nor free to move in all directions, because of their adsorption on to the fibre surface.

As a result of these limitations, the interphase material may be viewed as a region with variable properties. According to the "parabolic" model, the elastic modulus and Poissons ratio variations within the interphase are given by equations [15]:

$$E_i(r) = \frac{E_f - E_m}{(r_i - r_f)^2} r^2 - \frac{2(E_f - E_m) r_i}{(r_i - r_f)^2} r + \frac{E_f r_i^2 + E_m r_f^2 - 2E_m r_f r_i}{(r_i - r_f)^2} \quad \text{(A1)}$$

$$v_i(r) = \frac{v_f - v_m}{(r_i - r_f)^2} r^2 - \frac{2(v_f - v_m) r_i}{(r_i - r_f)^2} r + \frac{v_f r_i^2 + v_m r_f^2 - 2v_m r_f r_i}{(r_i - r_f)^2} \quad \text{(A2)}$$

where f is the fibre, m is the matrix and i is the interphase.

Substituting the values of E_f, v_f, E_m, r_f, r_i, v_m, the equations reduce to:

$$E_i(r) = 2690.28r^2 - 2394.35r + 533.01 \quad \text{(A3)}$$

$$v_i(r) = -9.72r^2 + 8.65r - 1.57 \quad \text{(A4)}$$

The equations represent a quadratic variation of interphasial properties, which may be seen in the Figs 6 and 7.

Acknowledgements

Dr N. Melanitis is thanked for performing the experimental work described in this paper. One of us (RBN) would like to thank Professor George C. Papanicolaou for useful discussions.

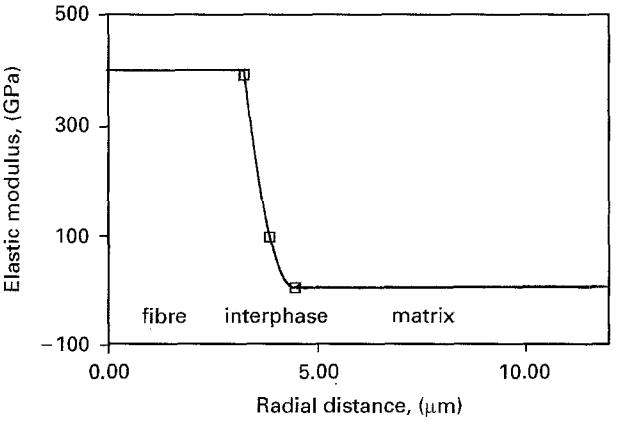

Figure 6 Variation of elastic modulus with radial distance.

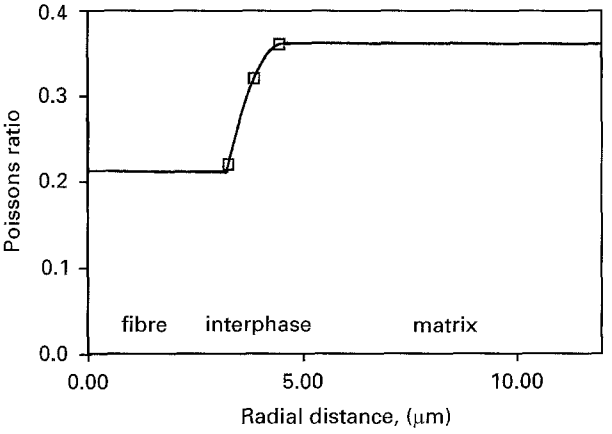

Figure 7 Variation of Poissons ratio with radial distance.

References

1. H. L. COX, *Brit. J. App. Phys*, **3** (1952) 72.
2. H. JAHANKHANI and C. GALIOTIS, *J. Comp. Mat.* **25** (1991) 609.
3. N. MELANITIS, C. GALIOTIS, P. L. TETLOW and C. K. L. DAVIES, *ibid.* **26** (1992) 574.
4. F. J. GUILD, C. VLATTAS and C. GALIOTIS, *Comp. Sci. & Tech.* **50** (1994) 319.
5. C. GALIOTIS, *ibid*, **48** (1993) 15.
6. C. VLATTAS and C. GALIOTIS, in "Developments in the Science and Technology of Composite Materials", ECCM-5, edited by A. R. Bunsell, J. F. Jamet and A. Massiah (European Association of Composite Materials, Bordeaux, 1992) p. 415.
7. C. GALIOTIS, *Comp. Sci. & Tech.* **42** (1991) 125.
8. N. MELANITIS and C. GALIOTIS, *Proc. Roy. Soc London, Series A*, **440** (1993) 379.
9. N. MELANITIS, C. GALIOTIS, P. J. L. TETLOW and C. K. L. DAVIES, *J. Mater. Sci.* **28** (1993) 1648.
10. D. K. JONES and A. T. DIBENEDETTO, in "Deformation and Fracture of Composites-3", University of Surrey, 27–29 March 1995 (The Institute of Materials, London, 1995) pp. 86–95.
11. A. T. DIBENEDETTO, *Comp. Sci. & Tech.* **42** (1991) 103.
12. A. PAIPETIS and C. GALIOTIS, *Composites* (submitted.)
13. A. BUSSCHEN and A. P. S. SELVADURAI, *J. Appl. Mech*, **62** (1995) 87.
14. M. R. PIGGOTT, *Comp. Sci. & Tech.* **42** (1991) 57.
15. P. S. THEOCARIS, E. P. SIDERIDIS and G. C. PAPANICOLAU, *J. Reinforced Plast. & Comp.* **4** (1985) 396.

Received 26 May
and accepted 15 December 1995